Biological reactor retrofitting using CFD-ASM modelling

J. Climentª, L. Basieroᶜ, R. Martínez-Cuencaª, J.G. Berlangaᶜ, B. Julián-Lópezᵇ and S. Chivaª+

[a,b] UNIVERSITAT JAUME I, Department of Mechanical Engineering and Construction and Department of Inorganic and Organic Chemistry, Av. Vicent Sos Baynat, s/n 12071 Castellón (Spain), (E-mail: jcliment@uji.es, raul.martinez@uji.es, julian@qio.uji.es and schiva@uji.es corresponding author+)
[c] SOCIEDAD FOMENTO AGRÍCOLA CASTELLONENSE, S.A (FACSA), C/ Mayor, 82-84, 12001, Castellón (Spain). (E-mail: lbasiero@facsa.com, jgberlanga@grupogimeno.com)

Abstract: In recent years, the interest on modelling activated sludge (AS) systems by means of Computational Fluid Dynamics (CFD) techniques has significantly increased. This work shows a successful case study combining CFD hydrodynamics and biokinetic modelling. The hydrodynamics is analysed by using the Reynolds-averaged Navier-Stokes equation for incompressible non-Newtonian fluids and SST turbulence model. Biokinetics has been included into the CFD as transport equations with source and sink terms defined by the Activated Sludge Model nº1 (ASM1). Furthermore, a strategy for reducing the computational cost while maintaining accuracy of the results of these calculations has been proposed. This strategy is based on a two-step solver configuration and the definition of a variable timestep scheme. The resulting CFD-ASM approach permits a proper evaluation of denitrification in the anoxic tanks as well as the reproduction of nitrate and readily biodegradable substrate distributions. To demonstrate the strength of the proposed CFD-ASM, it has been used to evaluate the operation of a full-scale AS system and optimize its performance through changes in the biological reactor anoxic zone. The original configuration has been retrofitted and modified after detecting intrinsic defects on the fluid behaviour within the tank. This study has been assessed by analysing hydrodynamics in detail and validating the simulation results with tracer tests and flow velocity measurements. Substantial variations on the Residence Time Distribution have been confirmed when modifying the internal elements of the tank configuration: the wall-bushing and the stirrer positioning. As a result of this work, an influential short circuiting was corrected improving hydrodynamics and increasing mean residence time, all favouring denitrification efficiency. Outcomes of this study show the benefit of CFD when applied to AS tanks.

Graphical Abstract

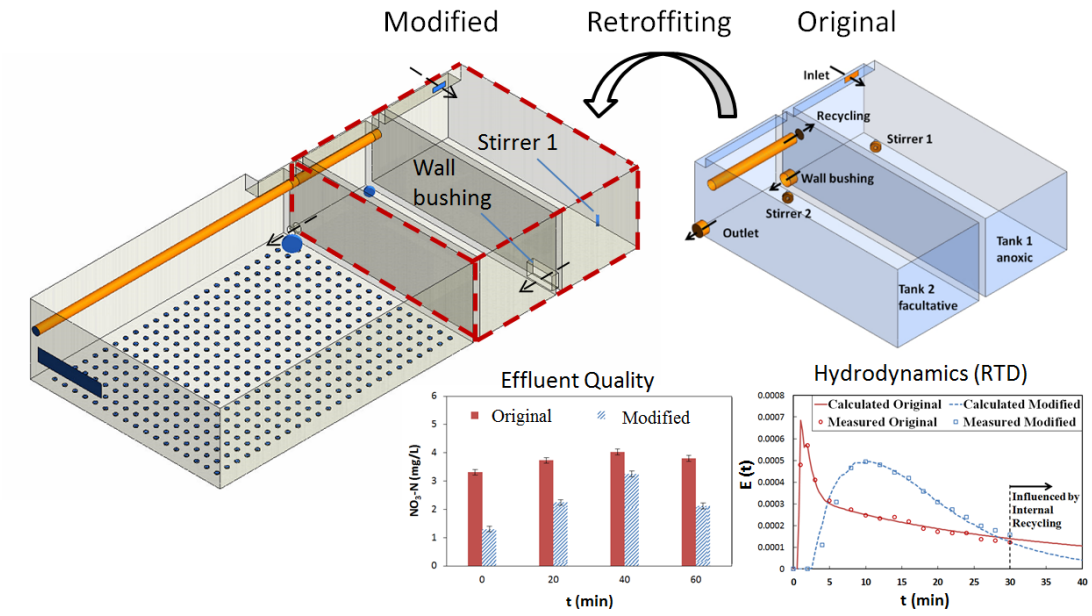

Highlights

- CFD models were used to retrofit a full-scale tank being validated experimentally
- A CFD virtual study was conducted to optimize the modified configuration proposed
- RTD was demonstrated to be strongly influenced by modifications over the internal elements within the tank
- A strategy of calculation was implemented to reduce computing time of simulations
- CFD-ASM models allowed to evaluate the improvement of fluid behaviour and denitrification efficiency

Keywords: CFD; ASM1; Denitrification; RTD; Anoxic; Full-scale

1. Introduction

The Modified Ludzack-Ettinger (MLE) biological reactor is a commonly used nutrient removal configuration, typical of municipal wastewater treatment (WWT) plants, composed of anoxic and aerobic tanks. As known, this system represents one of the simplest configurations to provide nitrification-denitrification with greater efficiency [1]. This increase in efficiency comes from two main factors: recovering lost oxygen, potentially up to 63% of the energy expended in nitrification, and alkalinity, about half of the lost through the nitrification is recovered when nitrate is used as electron acceptor of readily biodegradable organic substrate [2]. Denitrifying bacteria prefer to use molecular oxygen, but if the environment contains less than 0.3 to 0.5 mg/L of dissolved oxygen (DO), they will cleave the oxygen from nitrate-N molecules to oxidise carbon compounds (e.g., BOD)[3]. Hence, sufficient amounts of substrate must be ensured in anoxic conditions to carry out the denitrification process and thereby saving aeration energy consumption of the activated sludge (AS) system.

The main disadvantage of the MLE reactor configuration is that the effluent will always contain appreciable quantities of nitrate-N because nitrification occurs in the last bioreactor [4]. Consequently, the adjustment of the internal recycling ratio, which provides nitrate to the anoxic zone, is a critical operational parameter. As this case study, a common mode of operation consists on setting relatively high internal recirculation rate in order to maintain effluent under control. But, high recycling ratio causes strongly influence on the retention time of the anoxic tank, decreasing the denitrification efficiency. Accordingly, if the mean residence time of the anoxic tank is not enough, the aerobic tank must be often operated stopping aeration to provide (sufficient) further anoxic volume.

Mean residence time is a variable of paramount importance which should be well-known, and not assumed as the theoretical hydraulic retention time which frequently entails a poor approach. In this regard, Residence Time Distribution (RTD) that describes the amount of time a fluid element could spend inside the reactor is commonly used as an experimental source of knowledge giving useful information about hydrodynamics and mean residence time. Even though it is costly and not quite accurate when large-volume tanks are examined, RTD allows quantitative measurement of mixing, and what is more important the determination of the potential for pollutant removal [5]. It is possible to obtain crucial hydrodynamic information of AS systems from Computational Fluid Dynamics CFD tools providing deep knowledge of the fluid behaviour [6]. As shown in this study, CFD techniques allow to modify the shape of the RTD curve changing the internal elements within the tank [7]. The literature offers numerous examples of CFD tracer studies to reproduce fluid pattern and calculating mean residence time, dead volume, mixing, short-circuiting,

etc. which must be validated experimentally mainly by means of RTD and flow velocity profiles [6-9].

Several commercial packages with different level of complexity are available for modelling WWT processes. Design and operation are frequently based on ASM [10] which are generally implemented on ideal hydraulic tank-in-series models; nevertheless, due to the shape and size of the tank units, there is definitely an effect of hydrodynamics on the efficiency of the pollution abatement[11,12]. In order to obtain a more accurate approach, hydrodynamic effects can be modelled by means of CFD, and ASM can be maintained to reproduce the nutrient removal process. Thus, with the purpose to perform the simulations, it is possible incorporating ASM equations in the CFD code. The usual solving strategy is based on two steps; at the first step the hydrodynamics is solved, and secondly, from the velocity field as a known variable, ASM model is solved as a convection-diffusion problem for a set of transport equations, one for each species, where ASM terms are included as sources [12–15]. Authors agreed that successful modelling of the hydrodynamics facilitates the development of a complete model [13,15], being the CFD more powerful use to simulate integrated physical, chemical and/or biological processes involved in WWT design and operation, but to date, it should be understood as a supportive tool for unit processes design and troubleshooting [16,17].

In this paper authors want to exhibit the use of CFD to model a real bioreactor with malfunctions and its validation against experimental measurements. The results obtained by the validated model have been analysed and a new improved design has been developed using CFD. That new design was performed in the real WWTP, and further and more detailed experimental data were obtained to check the proposed modification and the CFD model itself.

This study deals with a faulty hydrodynamic performance of the biological reactor consequence of an influential short-circuiting detected in its design configuration (Original configuration). This direct flow between the wall-bushings, which were located facing each other, short-circuited the current flux in the second anoxic tank. In order to improve the performance, a new configuration (Modified configuration) was proposed by changing the locations of the wall-bushing and the stirrer as indicated in Fig. 2.

The outline of this work was divided into three different steps (Fig. 1). The two symmetrical wastewater treatment lanes (WWTL1, WWTL2) of the MLE bioreactor (Fig. 2) were used to carry out this study. Firstly, a CFD model (L1CFDo) was developed to study hydrodynamics in the Original configuration of WWTL1 (WWTL1o), being validated experimentally by means of tracer tests (I). Secondly, the CFD model was used to perform improvements of the fluid behaviour over WWTL1 (L1CFDmod) which was eventually retrofitted. After the full-scale modifications in WWTL1, the modified configuration (WWTL1mod) was validated using tracer tests and velocity measurements (II). Finally, CFD-ASM1 model for each configuration was developed calculating differences in denitrification performance, which were validated experimentally comparing WWTL1mod and WWTL2 (Original) (III). As a result from this study, we demonstrate that the retrofitted configuration WWTL1 (WWTL1mod) provides an effluent with higher quality compared with the unchanged WWTL2.

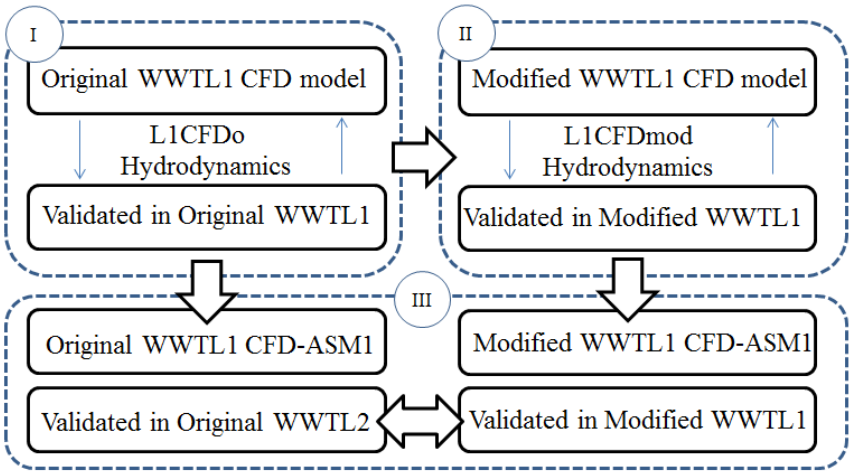

Figure 1. General outline of the study.

2. Materials & methods

The description of the reactor has a critical importance to obtain representative process dynamics when modelling the effect of local hydrodynamic phenomena on biochemical reactions [13]. This section starts with a full description of the biological reactor under inspection and introduces the proposed retrofitting configuration. Then, the experimental techniques used for model validations are presented along with the various locations at which data were acquired. Finally, the (novel) implementation of the combined CFD-ASM1 model is briefly described.

2.1 Description and operation of the biological reactor

This study has been conducted in a full-scale biological reactor of a WWT plant located in Vila-real (Spain). It was designed to treat a flow of 22 486 (m^3/day) (50 786 equivalent inhabitants). As shown in Fig. 2, its configuration consisted in a MLE activated sludge process composed by two symmetrical and separated WWTLs (WWTL1, WWTL2), set in parallel, each one composed of 3 tanks in a row. Each

tank was communicated to the next one by just one wall-bushing and equipped with one stirrer. Influent flow and external recycling from secondary settlers were previously mixed and equally distributed into the two WWTLs, feeding the first anoxic tanks where the DO is maintained lower than 0.1 (mg/L). Third tank was the only one able to form nitrate when operating under aerobic conditions. Internal recirculation stream for each WWTL returned mixed liquor from the Outlet, located after the third tanks, providing nitrate-N to the first tanks.

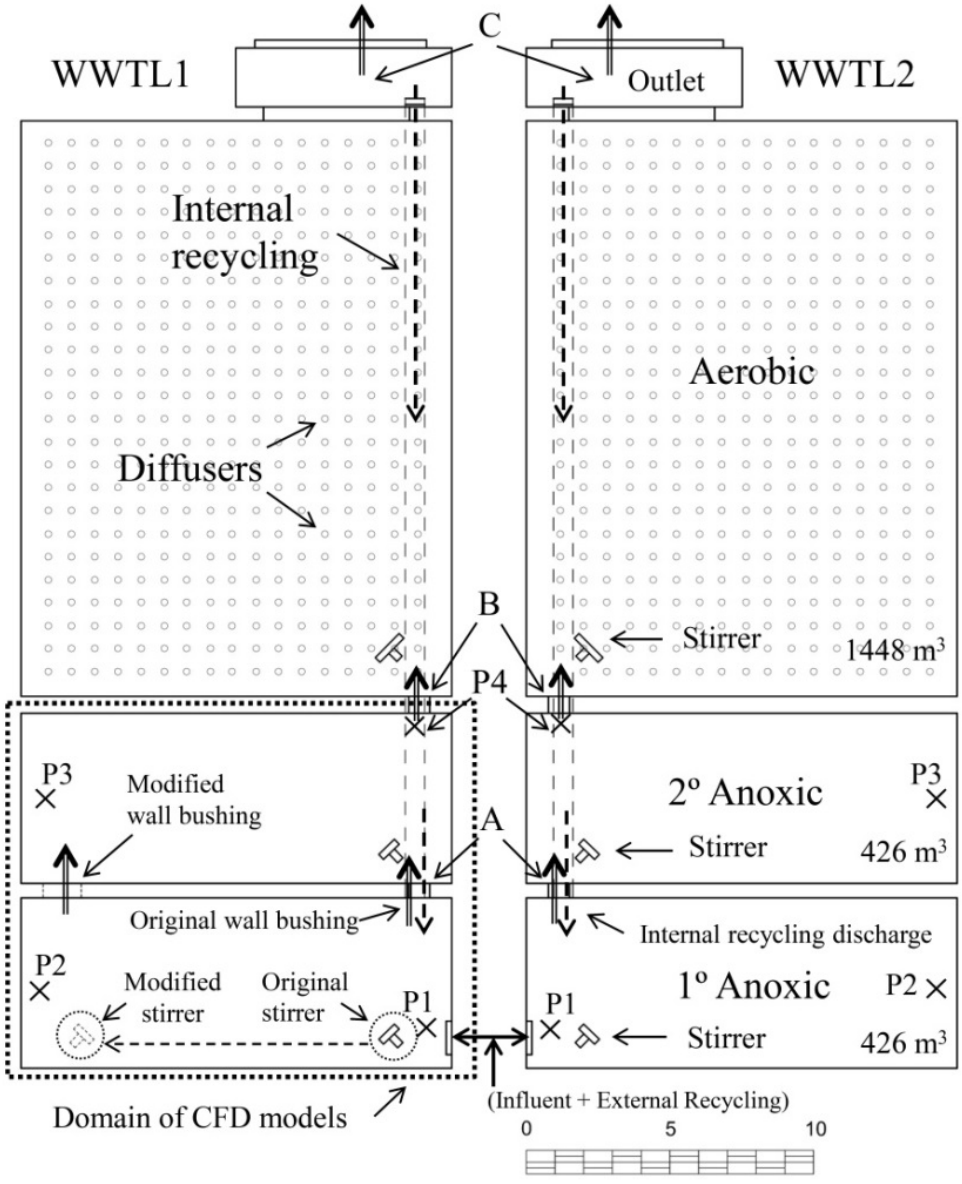

Figure 2. Plan view of the MLE biological reactor including both WWTLs.

The discharge point of the internal recycling within the first tanks was located just 2.5m above of the wall bushing between anoxic tanks (Original wall-bushing), whereas the following wall bushing, which communicated to the aerobic tank, was located in front of it causing a significant short-circuiting which induced hydrodynamics malfunctioning within both second tanks.

The biological reactor operates using intermittent aeration to promote both nitrification-denitrification in the aerobic tanks due to a high unintended accumulation of nitrates. This raises the difficulty in setting up the optimal aeration cycle time in order to guarantee reasonable concentration of nitrogen compounds in the effluent. That is why the third reactor is often needed to increase the denitrification volume added up to the anoxic tanks. The CFD study was focused on the first two tanks of the WWTL1, facultative tanks which always operated in anoxic conditions due to the poor denitrification efficiency achieved. As mentioned above and shown in Fig. 2, the modification consisted on retrofitting the wall-bushing and relocating the stirrer (Original to Modified).

2.2 Experimental measurements for CFD validation

This study started carrying out a first tracer test in the entire biological reactor, taking samples at different sensible points in each tank of both WWTLs for 24 hours, with the purpose to acquire broad knowledge about the fluid behaviour inside the tanks. Fluorescein sodium salt was selected as a dye tracer due to its advantageous performance, particularly when fairly high numbers of samples are needed. From these experiments, the RTDs were obtained at the outlet of each tank (A, B, and C in

Fig. 2) and at the sidestreams (internal and external recirculation), with the aim of analysing the flow pattern and quantifying the influence of the internal recycling over the mean residence time of the anoxic zone. In addition, as other authors suggested [9], a tracer sorption test was conducted to ensure its photochemical stability as well as its low adsorptive potential at values of pH above 7.

Dye tracer was introduced at the influent following a "pulse" as the injection method. Tracer concentration at the outlet point of the second anoxic tank (P4 in Fig. 2) was measured with a sampling interval of 2 min. Samples were processed with a fluorescence spectrophotometer *Varian Cary Eclipse* set at 491.5 nm excitation wavelength and a sample detector PMT voltage of 820 volts. The fluorimeter was calibrated using the effluent as the zero point and as the dilutant for preparing the dilution samples to calibrate the equipment.

A high-resolution acoustic Doppler velocimeter *Vectrino Nortek*® was used to measure velocity in the first anoxic tank after the retrofitting; an aluminium structure anchored to the wall allowed moving the velocimeter inside the tank to measure 3D fluid velocity at different locations and depths. Velocity at the second anoxic tank was not measured because of its more complex accessibility.

Rheological tests were carried out with a *BOHLIN® CVO 120 HG (High resolution)* rheometer equipment to measure physical properties of activated sludge at 18ºC such as viscosity and yield stress. Double concentric cylinder rotational rheometer was used to obtain the flow curves, taking into account that the gap size (measuring gap: 1.99 and 2.73 (mm) was much larger, at least 10 times, compared to the particle size in suspension (until 0.14 mm) [18]. There were performed sensitivity tests of the sample at different initial Shear Stress with the purpose to measure with sufficient

precision at low velocity gradients and to detect the characteristic threshold stress of the pseudoplastic sample.

Finally, physico-chemical analyses were carried out to characterise the influent flow, the internal recycling and to determine state variables at four different locations (P1, P2, P3 and P4) for comparing both WWTLs and validating CFD models, not only for global predictions but also for more local estimation of the concentrations[12]. Samples of 500 ml were extracted from a specific depth (2.5m for P1, P2 and P3 and 4.5m for P4 corresponding to the wall-bushing). In order to asses denitrification performance, filtered BOD was measured following the procedure described in [19] whilst Hach-Lange® photometric kit was used to measure Nitrate (kit LCK339).

2.3 CFD Modelling

A combined CFD-ASM three-dimensional non-Newtonian single-phase approach was performed with the purpose of evaluating the influence of the two different geometries over hydrodynamics and its impact on the kinetic model. *ANSYS*® *Academic Research Release 16.2* software was used to perform the CFD model. Different simulations which are described in this section were run in ANSYS-*CFX* for Original and Modified configurations to accomplish these aims.

ANSYS- CFX is cell-vertex finite volume, coupled implicit, pressure based solution technique, solving pressure and velocity at the same time in the same matrix. This code uses a co-located (non-staggered) grid layout such that the control volumes are identical for all transport equations, using the discretization proposed by the Rhie-Chow approach. ANSYS-CFX uses an unstructured Finite Element based Finite Volume method, using shape functions, common in FE techniques, to describe the way a variable changes across each element. It is also a node based code, where the

solution variables are solved and stored at the centres of the finite volumes, or the vertices of the mesh.

The resulting mesh for the simulations was selected after a grid dependence procedure and discretization schemes; finally, a hexahedral dominant mesh with 238 730 nodes was performed to calculate the simulations by means of hexahedral elements of approximately 17 cm of edge. The guidelines detailed in CFX Best Practices Guide for Numerical Accuracy [20] were took into account, testing mesh dependence and discretization schemes. Then, a sensitivity analysis of the mesh confirmed the null impact of the mesh size element on the simulation results. In addition, mesh quality parameters (orthogonal quality and skewness) had been checked in the defined mesh. High orthogonal quality and low skewness values are recommended, 0.95-1 and 0-0.25, respectively. Specifically, orthogonal quality average of 0.95761 and skewness average of 0.19593 were obtained.

The Shear Stress Transport turbulence model developed by Menter [21] was selected. This model is widely used and very robust. It is a two-equation eddy-viscosity turbulence model that combines the k-ω turbulence model near the wall when the inner region of the boundary layer has a dominant effect and k-ε turbulence model in the free shear flow.

Mixed liquor transport properties were defined as a non-Newtonian fluid using the Herschel-Bulkley submodel (Equations 1 and 2) [22] which enriched the performance since viscosity variations due to velocity gradients were taken into account.

$$\tau = \tau_0 + K\gamma^n \qquad (1)$$

$$\eta = \frac{\tau_0}{\gamma} + K\gamma^{n-1} \qquad (2)$$

Where τ is the shear stress (Pa) , τ_0 is the yield stress (Pa), K is the consistency index $(Pa\ s^n)$, γ is the shear rate (s^{-1}), n is the flow behaviour index and η is the apparent viscosity of sludge $(Pa\ s)$.

Inlet and outlet boundary conditions were defined with mass flow rates whereas the free surface of the fluid was stablished as a free-slip wall.

Submersible mixers used for flow controlled mixing in large volumes, and the single performance parameter thrust (F) is commonly known to be the basis for mixing system design, along with a set of mixer positioning principles. The submersible mixers could be modelled in a detailed way using CFD, but it is too complex to be include in a wide plant model, instead, a simile is used to include as a momentum source, M (kg m^{-2} s^{-2}) [7], the mechanical momentum added by the mixer in the system, in the same mixer geometrical location.

According to the technical sheet of the manufacturers, the following expressions were used to calculate the momentum sources. Subsequently, velocity measurements were conducted to calibrate more accurately this parameter.

$$q = C\ D \left(\frac{F}{\rho}\right)^{1/2} \qquad (3)$$

$$M = \rho \left(\frac{q}{D}\right)^2 \qquad (4)$$

Where q is the fluid flow propelled (m^3/s), C is a constant parameter, D is the diameter of the stirrer (m), F is the thrust force (N) and ρ is fluid density ($kg\ m^{-3}$).

The ASM model was implemented including an extra transport equation for each additional variable:

$$\frac{\partial}{\partial t}(\rho.\varphi_i) + \nabla.(\rho.U.\varphi_i) = \nabla.\left[\left(\rho.D_{\Phi}. + \frac{\mu_t}{Sc_t}\right)\nabla\varphi_i\right] + S_{\varphi_i} \qquad (5)$$

Where U is the fluid velocity ($m\ s^{-1}$), ρ is the mixture density ($kg\ m^{-3}$), Φ is the concentration of the i variable ($kg\ m^{-3}$), $\varphi = \Phi/\rho$ is the conserved quantity of i variable per unit mass of fluid, Sc_t is the turbulence Schmidt number, μ_t is the turbulence viscosity term in Pa s, D_{Φ} is the kinematic diffusivity ($m^2\ s^{-1}$) and S_{φ_i} is a volumetric source term ($kg\ m^{-3}\ s^{-1}$) that embeds the biochemical reactions.

Manifold simulations with different aims described below were performed over several configurations of the anoxic tanks with the objective to improve hydrodynamics and, consequently, nutrient removal efficiency.

2.3.1 Tracer runs in transient state

Dynamic simulations were run for 30 min being the mass flow rates defined as constants (Table 1). This assumption was made because the influent flow represented about the 15% of the total mass flow rate entering to the domain and it presented a low variation (< 5%) during the experimental measurements period. RTD was

calculated following the tracer concentration at the outlet of the anoxic zone (P4), and compared with experimental results for both configurations [23].

Table 1. Main parameters of CFD validation by means of "short tracer tests"

Mass tracer (g)	500
Q influent (m^3/h)	417
R internal (m^3/h)	1 570
R external (m^3/h)	541

The tracer was defined as an additional scalar field by means of a transport equation setting the tracer molecular diffusivity of 5.1 10^{-9} m^2 s^{-1}[24] and the Schmidt number of 0.9 [7,25]. The pulse of mass tracer at the inlet was modelled by properly using step functions.

2.3.2 RTD calculation in steady state

Tracer transport method [26] is a feasible way to perform a comparative study among different options. This implies a simple definition of residence time and can be run in steady state, which entails reducing efforts in terms of computing time and complexity of the simulations. This method was used to study and to select the optimal Modified configuration.

Mean residence time from the simulations is calculated by means of an additional scalar field, t_m (s), that is described by the following transport equation (Eq. 6).

$$\sum_j \left[\frac{\partial}{\partial x_j}\left(U_j t_m - D_{tr}\frac{\partial t_m}{\partial x_j}\right)\right] = 1 \qquad (6)$$

where D_{tr} (m^2 s^{-1}) stands for the total diffusivity of the tracer in the fluid and U_j the velocity components.

Simulations were carried out in steady state calculating the value of the t_m from the Eq. 6 to obtain the field of the mean residence time in the domain. Several wall-bushing features were studied depending on its shape and its flow cross section size. Hence, a criterion based on the fluid behaviour consisting on maximizing the mean residence time was defined. From this comparative analysis, the optimum performance to carry out the full-scale modification of WWTL1 was selected.

2.3.3 CFD-ASM runs

ASM1 equations were taken from [10]. Therefore, 8 processes and 13 state variables were introduced as volumetric scalar fields (table 2) that were transported following the Eq. 5.

Most of the values for the kinetic and stoichiometric coefficients of the mathematical model were defined as default values for 20ºC [27]. Even so, some parameters were determined by respirometry.

Table 2. State variables at initial and boundary conditions. (mol/m^3)*

State variable	Inlet (influent + External recycling) (g/m^3)	Internal Recycling (g/m^3)	Initial Conditions (g/m^3)
S_I	20	20	20
S_S	172.4	38	12

X_I	152.8	152.8	152.8
X_S	207.4	68	52
$X_{B,H}$	2745	2745	2745
$X_{B,A}$	305.6	305.6	305.6
X_P	562	562	562
S_O	0.5	0.8	0.01
S_{NO}	2.1	7.2	4
S_{NH}	51.6	3.7	7.6
S_{ND}	7.4	1	2
X_{ND}	2	2	2
S_{ALK}*	4.4	4.4	4.4

Table 2 shows the values of the state variables used as boundary conditions and for the initialization of the transients; they were experimentally measured from the settled influent and both recycling streams. Despite the fact that state variables were not defined with dynamic boundary conditions, they were calculated in transient state in order to study their time evolution. Moreover, with the goal of ensuring that global balances were met after the simulation, a target imbalance about 0.3% was stablished for the conservation of each state variable, being achieved results lower than typical default value recommended of 1% [20].

2.3.4 Saving computational time

Typical time steps for the iterative resolution of hydrodynamics are of the order of the millisecond, depending on flow speed and mesh refinement through the Courant number. Given the RTDs corresponding for MLEs and the slowest reaction times for

the biochemical processes involved take place at time scales way over the hydrodynamic timescale, their resolution would require a huge number of time steps. In order to reduce the number of time steps needed for the calculations, one can isolate both phenomena and resolve the corresponding equations separately. In practice, the number of iterations required for a proper resolution, and therefore in computational time, has been reduced by using a two-fold solving strategy, it results convenient to isolate both phenomena and resolve the corresponding equations separately.

As a first proposal for the reduction of the calculation time, we noted that the fluid pattern in the anoxic tanks could be considered constant as there was no aeration (the hydrodynamics only depended on the stirrers momentum and incoming streams flowrates, which both are set constant in normal working conditions). These tanks have a strong fixed recycling stream, then the effect of the influent flow temporal evolution is quite limited. We could assume the hydrodynamic variables are constant over a long period of time.

Then, as the hydrodynamics is not generally affected by biokinetics in these processes, transient simulations can be split in two steps. In the first one, hydrodynamics was calculated in steady state by using a proper time step. No biochemical reactions were allowed in this step. In the second step, the transport equations for the biokinetics were solved by using the flow fields obtained in the previous step, which remained constant, i.e., no flow equations were solved throuout this step. This strategy has an important advantage; it is possible to solve the biokinetic evolution over a long period of time with a non-expensive computational cost in scenarios where the hydrodynamic remains essentially constant.

A second proposal for the reduction of computation time is based on the use of a variable timestep that changes as the simulation advances. Given the structure of the biokinetics source terms [28], one can expect that the reactions take place faster in the beginning and their speed reduces as the reactions advance until they reach the equilibrium. Consequently, the solver was fed with a time step increasing with the iteration number, providing more accuracy, shorter timesteps, at the initial timesteps to ensure a proper convergence and prevent from overflow errors.

The variable timestepping proposed follows a geometric series, $t_s = t_o r^s$, where s stands for the iteration number, t_o the initial time step and r the time common ratio. Then, the total simulation time is given by the expression:

$$T = \sum_{s=1}^{S} t_s = t_o \frac{1 - r^S}{1 - r} \qquad (7)$$

Where S and T stand for the total iteration number and total time, respectively. In practice, the initial timestep is set to be equal to that of the hydrodynamic part. Then, the common ratio is calculated according to the desired number of iterations (or computational time). The performance of this new approach will be tested and compared to constant timestepping schemes in section 3.2.

2.3.5. Rheological properties

The mixed liquor has a non-Newtonian behaviour, and a rheological study was performed to characterize the fluid [23]. The experimental data has been included as supplementary material. From this, the Herschel-Bulkley model was selected to

provide a complete description of the pseudo-plastic behaviour of the fluid [22]. The fitting parameters resulted τ_0= 0.00883 Pa; K= 0.01932 $Pa\ s^n$; n=0.6262.

In order to ensure a reliable experimental dataset, preliminary preparation of the sample was carried out to guarantee homogeneity of mixed liquor when measuring; it was induced a Shear Stress of 0.5 Pa for 30 s and to stand for another 30 s before to start measuring. Since the total suspended solids percentage in liquid is low (< 1%), The fluid in the CFD model was defined as a non-Newtonian single phase to reproduce changes in physical fluid properties under different velocity gradients.

3. Results & Discussion

3.1 Hydrodynamics

3.1.1 Tracer tests and simulations

The tracer concentration-time curves, C(t), obtained from the first tracer test are shown in Fig. 3. On one hand, C(t) curves measured at the outlet of each WWTL (point C in Fig. 2) showed that overall both lanes corresponded to a similar hydrodynamic performance noticing that the maximum concentration of tracer was achieved at the same time. The marked peaks indicate short-circuiting as will be discussed later, whilst the shape of the curves for long times suggests that the flow pattern can be understood as completely mixed. On the other hand, C(t) obtained at recycling streams provided the performance of mass tracer returned to the first anoxic tank, thereby the peaks revealed the time that takes the maximum concentration flow to return through the sidestreams. From this, it was observed the strong influence of

the mass tracer recycled by internal recirculation over the tracer concentration measured at the outlet point (P4) of the anoxic zone. According to this, it was considered that mass tracer recirculated may not have impact on the tracer concentration measured at P4 until after 30 minutes. Thus, it was possible to define a total time of 30 minutes for the "short tracer tests" with the purpose to avoid recycling tracer material as boundary condition in the CFD simulations.

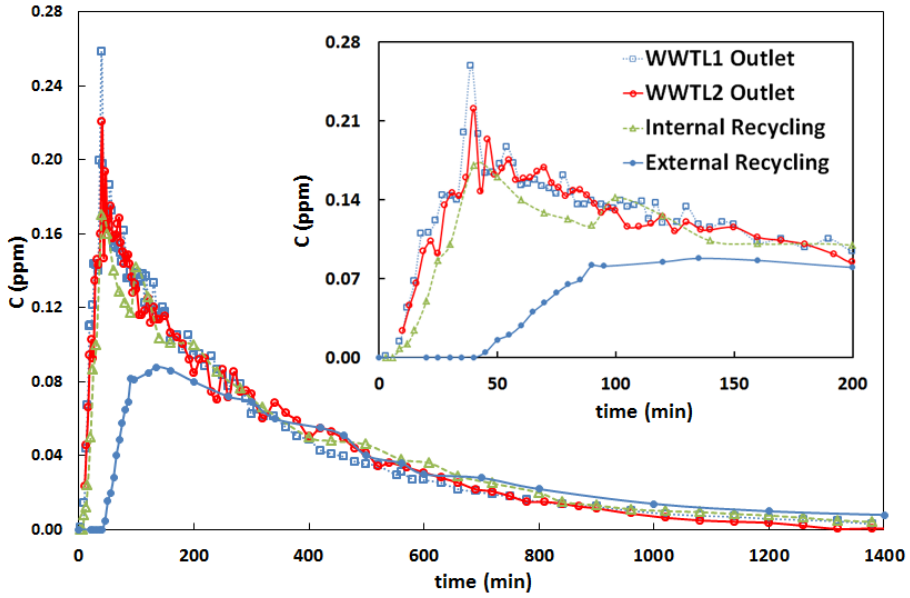

Figure 3. Comparison of C(t) curves measured at the outlet and at the sidestreams for the full test and detail of the initial part of the dataset.

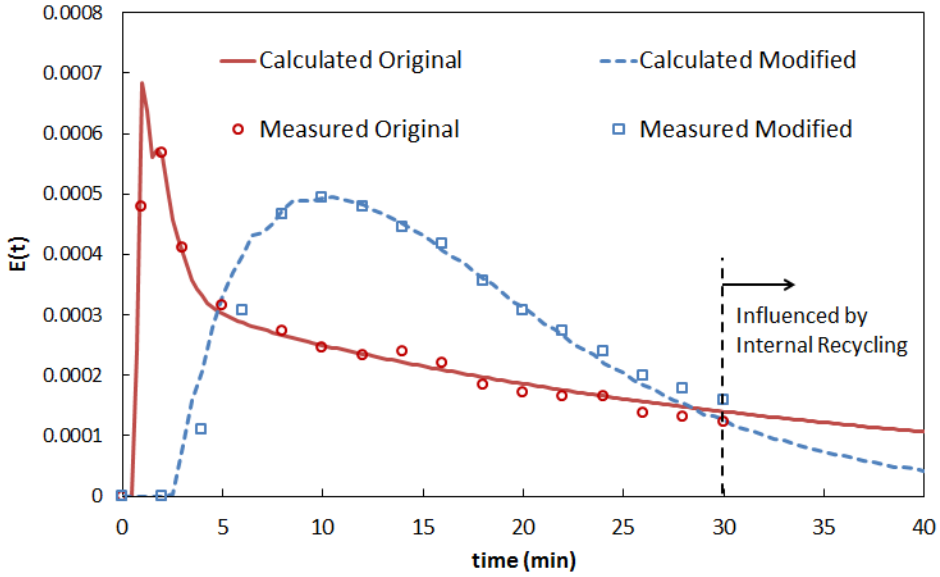

Figure 4. Comparison and validation of both RTD obtained in WWWT1 configurations: Original and Modified.

Figure 4 shows the residence-time distribution function E(t) at P4 for both the Original and Modified configurations. CFD model provided good results and fitting well with experimental data obtained from "short tracer tests". As expected, note that the CFD and experimental data start to differ significantly since minute 30, as the CFD model does not include recycling of tracer concentration. The hard peak in the Original configuration appears as a significant part of the inflowing tracer exited the tank in a time much shorter than the mean residence time, which further indicates the presence of a short-circuit. The curve corresponding to the Modified configuration indicates that there is no longer short-circuiting. Also, the full curve is displaced to the right side and smoothed out, leading to an increased mean residence time. Thus, this configuration provides an improvement of the global fluid behaviour in the tank.

Besides the visual inspection of short-circuiting and mixing from the shape of RTD curves in Fig. 4, where the improvement of the fluid behaviour is quite apparent, it is

often desired a quantitative criteria to better stablish a comparison. There are different methods available for analysing the results of tracer studies based on Levenspiel work [29], and not all of them provide useful information, for example, to parameterise short-circuiting [30].

Table 3 shows the main parameters used to compare analytically both configurations reporting the improvements provided by the retrofitting. Mean residence time was calculated as

$$t_m = \int_0^\infty t\, E(t) dt \ , \quad (8)$$

being

$$E(t) = \frac{C(t)}{\int_0^\infty C(t) dt} \ . \quad (9)$$

In order to calculate the number of tanks-in-series (N), one can start by defining the Normalised RTD Function E(θ) as

$$\mathrm{E}(\theta) = t_m E(t), \quad (10)$$

where θ is the normalized time $\theta = (t/t_m)$. In this approach, N is related to the normalized time at which the Normalised RTD is maximum, θ_{max}, by the relationship [30].

$$\theta_{max} = (N-1)/N\,. \qquad (11)$$

The parameters analysed are the theoretical hydraulic retention time, τ, the mean hydraulic residence time, t_m, the effective volume ratio (average retention time) calculated as t_m/τ, the reactor dead space volume calculated from (t_m/τ), V_d, the dimensionless time evaluated at maximum concentration, θ_{max}, and the number of tank in series, N.

Table 3. Main parameters of experimental RTD analysis

Case	τ (min)	t_m(min)	t_m/τ	$V_d(\%V)$	θ_{max}	N
Original	17.3	12.4	0.71	28.3	0.08	1.09
Modified	17.3	17.1	0.99	1.15	0.59	2.42

Modified configuration provided overall better hydraulic conditions than Original configuration since mean residence time increased by 38% approximately and the value of dead volume calculated decreased significantly. This dead volume calculated for the Original configuration should be interpreted as a rough indicator referred to a portion of volume partially isolated in the second anoxic tank consequence of the effect of the short-circuiting; it remained semi-stagnant with low turnover time. Results showed that the flow pattern of the Modified configuration provided more plug fluid behaviour than the Original configuration. That said, it is important to point out that calculations in Table 3 were made from experimental data values not beyond than ≈ 2 θ, therefore, without considering the entire tail of the RTD. The differences calculated between both configurations based on these parameters would have been lower if RTD tails had been taken into account [31].

In addition to the validation through global data, velocity profiles were measured at three points at five different heights of the first tank of the Modified configuration (Fig. 5) in order to reproduce hydrodynamics in detail. CFD model was validated by means of a comparison of calculated and measured values at these specific locations offered in Fig. 6. Velocity profiles calculated showed good agreement with experimental data; velocity profiles measured exhibited a smoother behaviour than calculated. Velocity values were in the range 0.10 – 0.30 m/s depending mainly on the distance from the stirrer and the internal recycling. The most important issue in velocity calibration was to assess the parameter M in (Eq. 2) for the momentum of the stirrers and their location inside the tank. Both parameters governed the fluid behaviour along with internal recirculation flow in a second term.

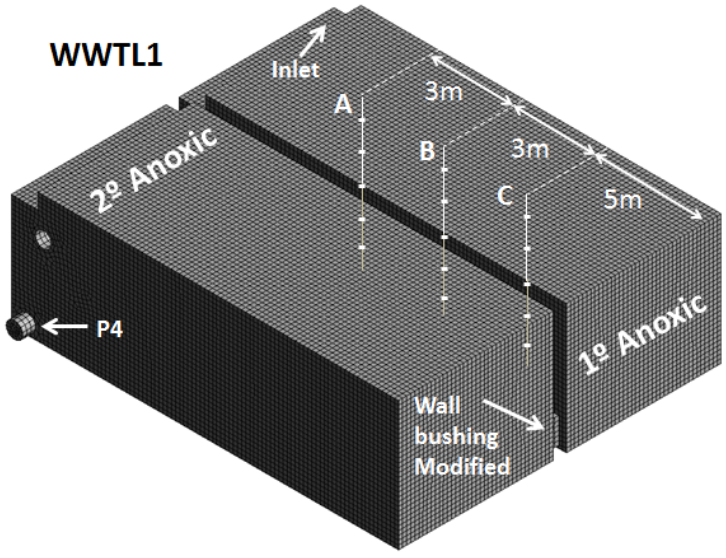

Figure 5. Mesh of anoxic zone and points of velocity measurements (A, B, C)

Each measurement was registered for 5 minutes in order to minimize the influence of rapid variations in flow velocities and to obtain representative hydrodynamic

behaviour. It is important to mention that the raw signals acquired by the velocimeter should be treated using a filter, in this case type Savizky-Sgolay (polynomial least-squares adjustment).

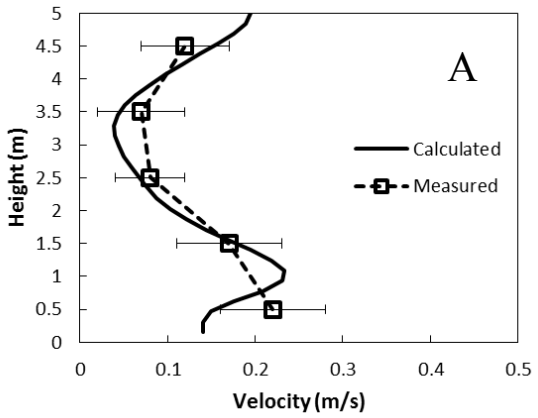

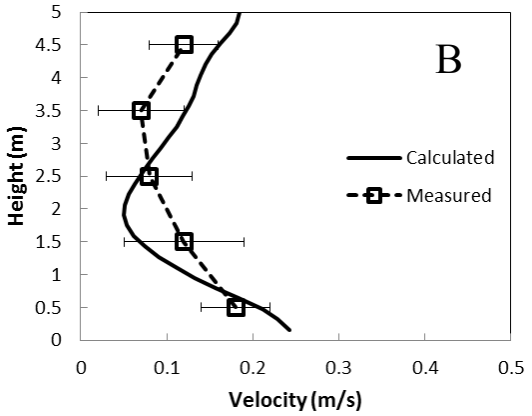

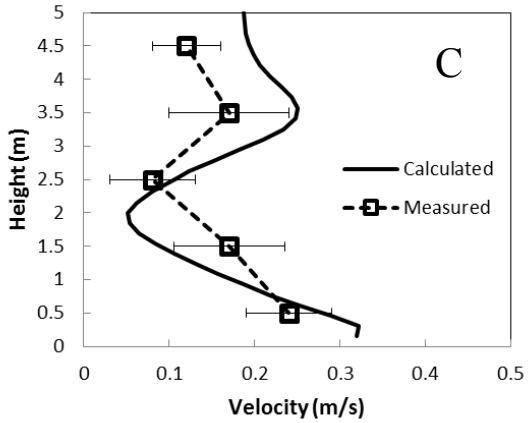

Figure 6. Velocity profile at a) position A b) position B c) position C

Streamlines and velocity of the fluid were calculated to describe the fluid behaviour. Figure 7 shows the streamlines revealing the faulty hydrodynamics performance in Fig. 7a as long as the improvement in the Modified configuration (Fig. 7b). Therefore, it is apparent that the existence of the short-circuiting in the Original configuration was not consequence of the poor mixing degree but because of the design configuration which provided the semi-stagnant portion of volume mentioned above.

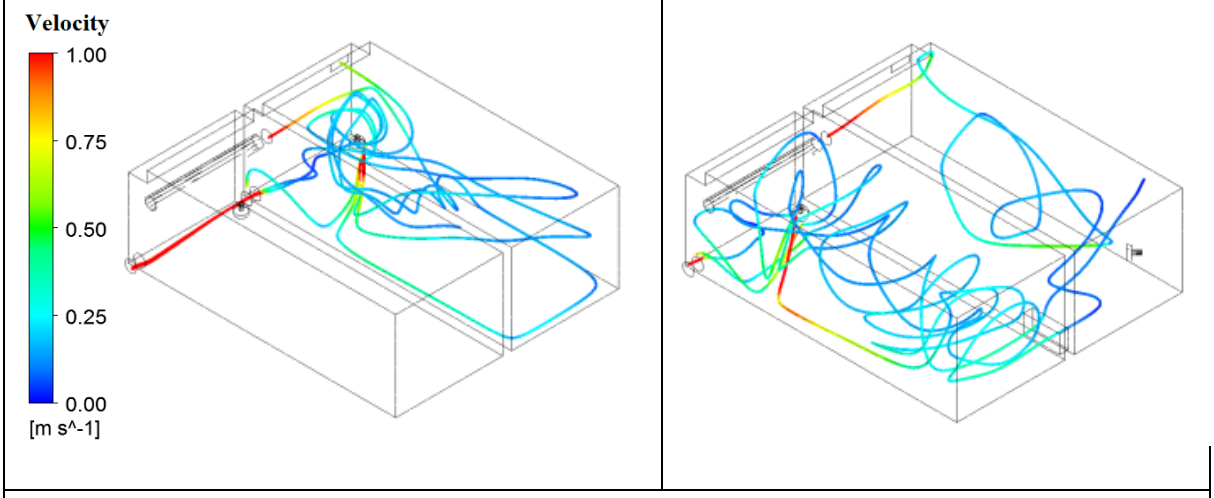

Figure 7. Streamline of a) short-circuiting at Original configuration. b) improved at Modified configuration

3.1.2 Optimization study

Once Original configuration CFD model was validated, and the problem detected, and a possible solution proposed, several configurations were carried out in order to improve hydrodynamics. Assuming that an improvement in the fluid behaviour will provide a better performance of the biological nutrient removal process, biokinetics were not included to optimize the configuration proposed.

Besides tracer simulations run in transient state explained in section 2.3.1 and discussed above, RTD simulations were run in steady state. As explained in 2.3.2, an additional scalar field representing mean residence time, t_m,was included to study spatially this the mean residence time field [26]. An explanatory figure has been included as supplementary material representing the portion of fluid volume which contained values of t_m between 500s and the time when the fluid escapes from the anoxic zone at the original configuration, 680 s. As well as the figure 7 indicates, the Modified configuration removed the short-circuiting.

In order to optimize the performance of the Modified configuration, a virtual study is developed, consisting of several simulations. First, the influence of wall-bushing crossing section area (between 0.5 and 4 m^2) and shape (circular and rectangular) on the residence time and velocity field homogeneity is studied (see Table 4). Then, the optimal crossing-area and shape combination is used as a basis for a study on the stirrer positioning (6 positions as in Table 5) and its influence on the mixing efficiency of the tank. Finally, the optimal position is used as a basis for a study on the orientation of stirrer (3 angles). The angular orientation providing better mixing performance is then chosen as the optimal one.

Table 4. Description of the configurations tested to optimized the wall-bushing

Configuration	Geometrical shape	Crossing section (m^2)	Parameter (mm)
1	circular	0.50	Ø 800
2	circular	1.13	Ø 1 200
3	rectangular	1.13	1 130 x 1 000
4	circular	2	Ø 1 600

5	rectangular	2	2 000 x 1 000
6	rectangular	2	2 x (1 000 x 1 000)
7	rectangular	3	2 500 x 1 200
8	rectangular	4	2 500 x 1 600

The optimization of the Modified configuration was based on maximizing t_m and the fluid velocity homogeneity. As an example, Fig. 8 shows t_m variable represented over a plane located at 0.60 m height (wall-bushing crossing section). Slightly differences can be appreciated among the configurations. Thus, Figs. 8a and 8b show the improvement when increasing the crossing section. A hardly noticeable difference can be appreciated between different crossing section shapes enclosing the same flow area (Figs. 8c and 8d). A gradual increase of the crossing section was tested showing that there was an optimum configuration, since above 2 m^2 crossing section a t_m variable field was worsening instead of getting better (Figs. 8e and 8f). The latter shows an undesirable effect of the fluid induced by the wall bushing. It consisted of zones with upper t_m values, which would correspond to be closer to the Outlet, located behind zones with lower t_m values.

a)	b)

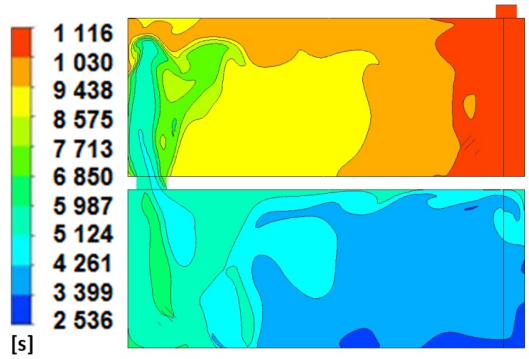

c)

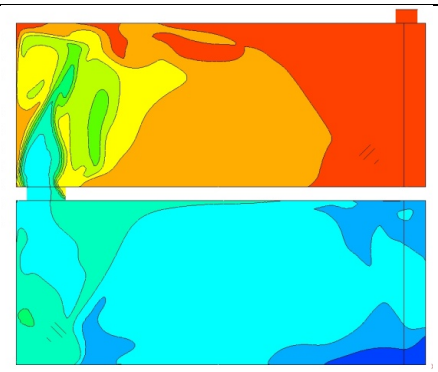

d)

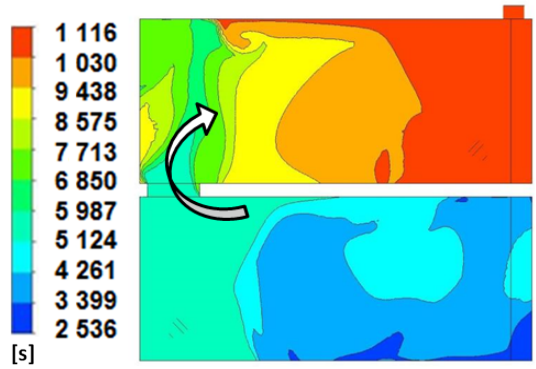

e)

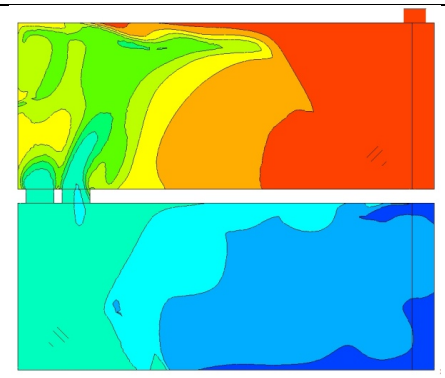

f)

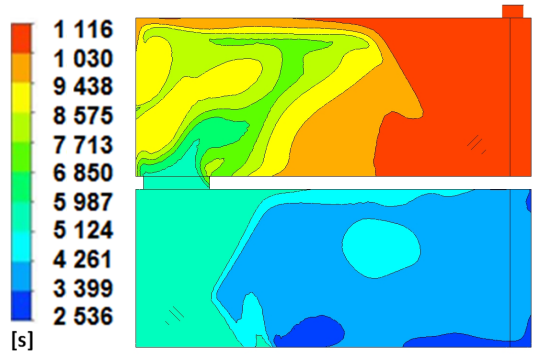

Figure 8. Horizontal cross-sections for t_m variable in a) configuration 1, b) configuration 2, c) configuration 5, d) configuration 6, e) configuration 7 and f) configuration 8

In order to provide a more detailed description of the hydrodynamics inside the tanks, fluid velocity fields are shown for the different configurations. It can be noticed that a more homogeneous velocity field is achieved as the crossing section increased.

Comparative fluid velocity profiles between configurations have been plotted over the dashed lines drawn in Figs. 9 and 10, being included as supplementary material. They show that there is a noticeable local reduction of fluid velocity when the crossing section increased from 0.5 m^2 to 1.13 m^2 (Fig. 9) and also up to 2 m^2 (Fig.10), and no substantial differences has been found depending on the number of wall-bushings (one or two) for 2 m^2 configuration (Fig. 10).

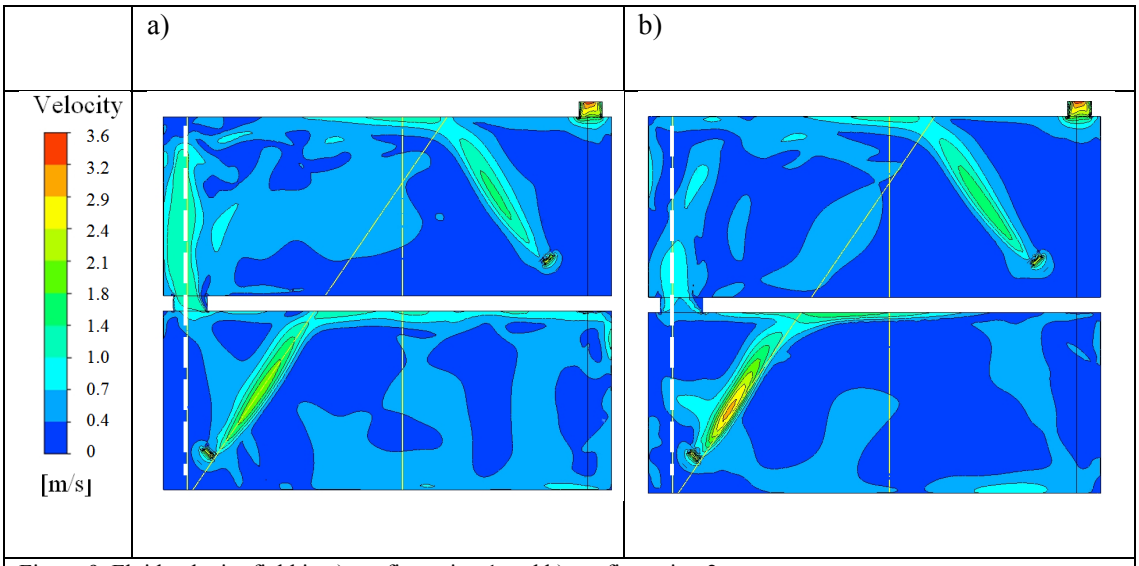

Figure 9. Fluid velocity field in a) configuration 1 and b) configuration 2.

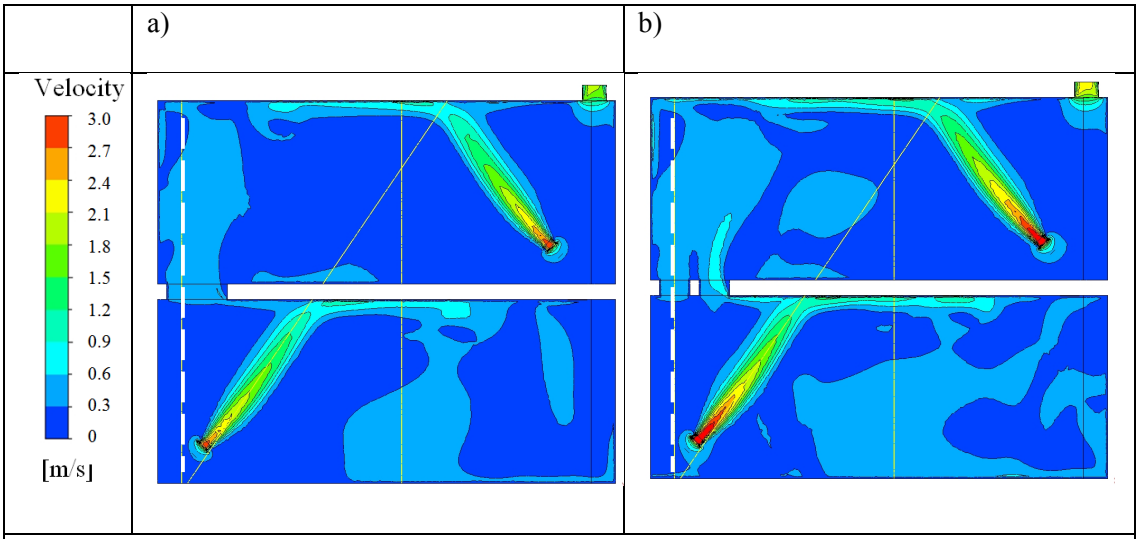

Figure 10. Fluid velocity field in a) configuration 5 and b) configuration 6.

After the steady state simulations, an optimal crossing section of 2 m^2 with a rectangular wall-bushing shape (configuration 5) was selected. This configuration improved hydraulic efficiency indicating that more effective use of available tank volume was occurring (maximizing t_m variable). Also, the resulting local velocity after the wall-bushing is reduced leading to an enhanced homogeneity of the fluid velocity field.

A comparative study was conducted to relocate the stirrer of the first tank according to its position and its angle. Transient simulations were performed reproducing the same procedure of the "short tracer tests" mentioned in section 3.1.1 for 5 positions and 3 different angles. The purpose was to evaluate the stirrer mixing efficiency by means of the tracer concentration through the wall-bushing depending on these two factors. Tracer concentration was calculated as an average of the crossing section in time and it was used as the main indicator for the following approach: the higher mixing efficiency, the lower the tracer concentration exiting the first tank.
We have defined the Reference configuration under the assumption that the proper location for the stirrer (Modified stirrer) should be symmetrical from the initial one (Original stirrer). An explanatory figure has been included as supplementary material. The stirrer in reference case is therefore located at 0.70 m from the main wall (X direction), 1.5 m from the side wall (Y direction), and 1.2 m from the bottom (Z direction). Then, in order to study variations around this reference, 5 additional locations were proposed. Table 5 summarizes the relative locations of these new positions.

Table 5. Description of the different locations tested

Location	Relative position X (m)	Relative position Y (m)	Relative position Z (m)
Reference	0	0	0
Ahead	0.5	0	0
Up	0	0	0.3
Down	0	0	-0.3
Right	0	0.6	0
Left	0	-0.6	0

Figure 11a shows the evolution of tracer concentration over time calculated at the crossing section for the different spatial locations described in table 5. It is appreciated the different tracer performance obtained through the wall-busing after the pulse of mass tracer at the inlet. All cases presented a similar initial time, defined as the time from which tracer starts exiting the first tank. The maximum tracer concentration values are achieved for Up and Left relative positions of the stirrer which correspond to a reduced efficiency in terms of mixing. On the other hand, a much better mixing performance is achieved by Down and Right relative positions since lower tracer concentration values escaping the first tank are obtained. The Right position was finally chosen due to it presented low values of tracer concentration and the maximum value of the initial time.

a) b)

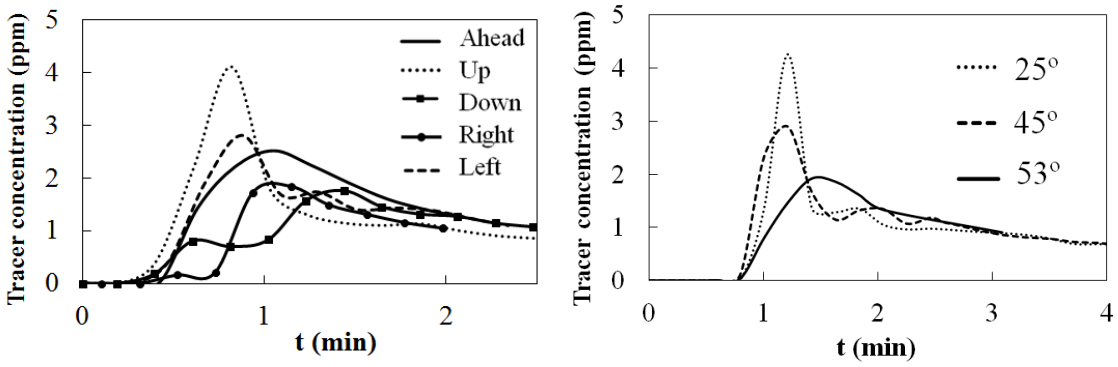

Figure 11. Tracer concentration calculated at the crossing section for different a) positions and b) angle

Figure 11b exhibits the importance of the angle when relocating the stirrer. The most acute angle provided a sharp peak related to an unintended high tracer concentration exiting the first tank. This peak was reduced when opening the angle of the stirrer respect to the Main wall. It is worth to notice that real angles were tested since the mast of the stirrer in the real plant had limited positions. It was concluded that the angle of 53º provided the lowest peak being potentially a good option to provide a much better mixing performance.

To conclude with the optimization study, Fig. 12 shows the comparison of the fluid velocity field between the Original and the Modified configuration after the optimization study. The wall-bushing was retrofitted removing the short circuiting and providing a homogeneous fluid velocity field; the 2 m^2 rectangular shape option was selected. Moreover, the optimal configuration, corresponding to the stirrer placed in Right position at an angle of 53º, provided a mean residence time increased by 38% over the original anoxic zone. Also, maximum tracer concentration was reduced by 30%. This optimal configuration will be referred to as Modified configuration from now on.

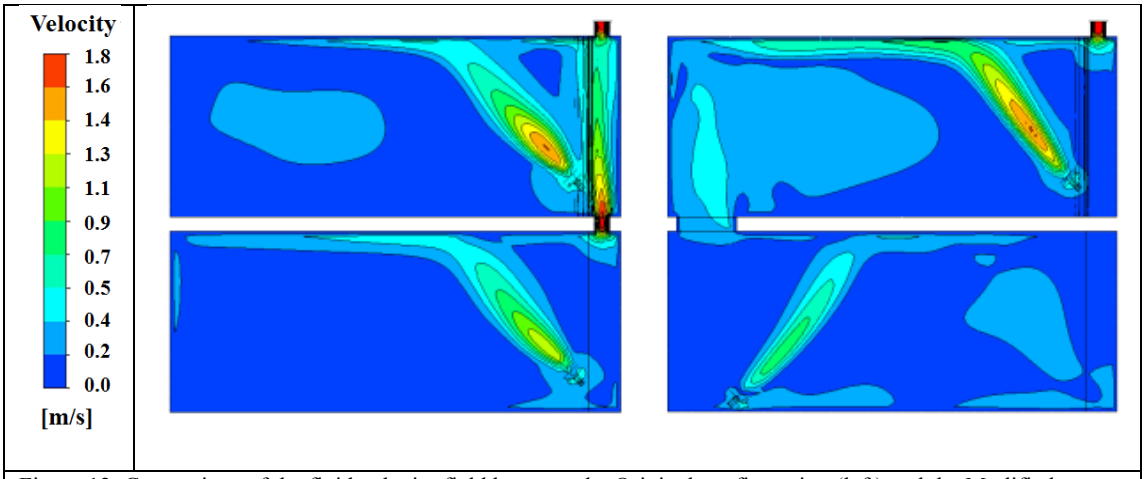

Figure 12. Comparison of the fluid velocity field between the Original configuration (left) and the Modified configuration (right)

3.2 Optimization of timestep selection

Typically, the calculation of full-scale CFD-ASM models implies high computing times. As mentioned in Section 2.3.4, simulations were run in two steps with the purpose to reduce computational costs, solving hydrodynamics in the first step, and kinetics in the second one. Furthermore, a timestep sensitivity analysis over the second step of the simulation was performed with the aim to obtain a maximum value of timestep which would provide good accuracy in CFD results. In order to do that, the evolution of the state variables was solved several times by employing different timesteps for each run. All runs shared the same velocity field, as a single steady state solution was used to feed the transient with frozen hydrodynamics. The evolution of the state variable value in time for different timesteps has been plotted and included as supplementary material. It was found that there was no significant difference on the resulting state variables (lower than 0.1%) when the timestep is kept below 1s. When this value is increased up to 100 s, the simulation time is conveniently reduced, but leading to deviations of approximately 5% (see Table 6) at the end of the simulation. Further increase of the timestep results in faster computations but at higher deviations.

It was also noted that the numerical imbalance of the partial differential equations (PDEs) increased over 5% for some state variables, thus exceeding the aforementioned 1% maximum recommendations. Also, the initial part of the transient shows actually very different values, leading to huge errors in the computations in the early times of the simulation.

Given that the value for the state variable tends to similar values for every timestep studied (within a range of 10%), but the differences in the earlier steps of the simulations can be huge, it makes sense to use the variable timestepping procedure provided by (Eq. 5). Moreover, the resulting timestep evolution when an initial timestep of 1 second is used for the first iteration, total simulation time of 2 hours is desired, and a total number of 724 iterations is set. This information is included as supplementary material. This strategy of calculation was successfully applied to this case being especially useful for transient simulations with constant inlet conditions, but its application should be studied carefully for simulations with dynamic influent conditions.

Table 6 contains the parameters of interest from the feasibility of running simulations being the features of the PC as follows: Intel® Cores™ i7-3770 CPU 3.40 GHz 32.0GB RAM. It is appreciated that the variable timestep provided highest accuracy in a reasonable computing time.

Table 6. Comparison of the main features of simulation depending on the timestep

Timestep value	Number of iterations	Total computing time (h)	Error in steady state (%)
1 s	7200	28.24	reference

100 s	72	0.39	4.68
900 s	8	0.06	10.15
variable	726	2.86	0.003

3.3 Study of the denitrification process

The CFD-ASM model described in section 2.3 was used to calculate and compare the denitrification performance for both configurations. Nitrate (Sno) and readily biodegradable organic substrate (Ss) concentrations and their consumption rates were selected to evaluate denitrification process.

After the full-scale modification in WWTL1, permanent unbalanced denitrification efficiency was observed between both lanes; Modified WWTL1 was favoured over the Original WWTL2 in terms of effluent quality due to its better hydrodynamics performance. Figure 13 shows the comparison between both WWTLs obtained for an equal continuous operational regime taking samples in time at the outlet of the aerobic tanks (point C in Fig. 2). Nitrate concentration of the Modified WWTL1 presented lower values than the Original WWTL2 being the average difference by 17%, with a maximum difference of 60%.

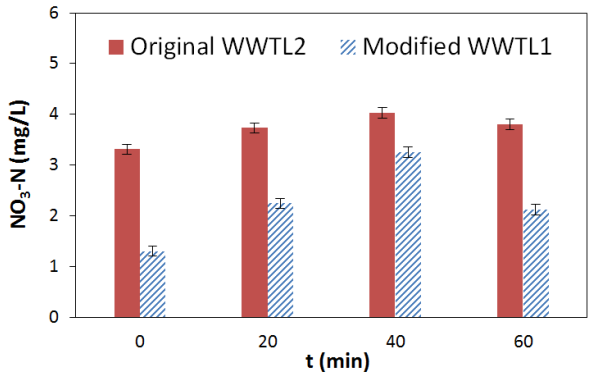

Figure 13. Comparison of Nitrate measured at different times at outlet of both WWTLs.

Moreover, experimental measurements were conducted within the both anoxic zones in order to validate CFD-ASM model and comparing both WWTLs. On one hand, a representative sampling volume was taken at four different control points located at 2.5m height inside both anoxic zones (P1, P2, P3 and P4 of Fig. 2). On the other hand, CFD-ASM1 results were calculated as an average concentration integrated over a specific bulk defined around each control point. Assuming the same distribution and composition of influent flow for both WWTLs, CFD-ASM1 models at Fig. 1 were performed defining the boundary conditions on equal terms for both configurations as described in section 2.3.3 table 2, except for the nitrate concentration at the internal recycling, which was adjusted because of the unbalanced state of the Modified WWTL1 being reduced by 17%. CFD results reproduced correctly main trends of pollutant concentrations within the tank (Figs. 14 and 15). In general, the tendencies provided by CFD-ASM1 models can be considered acceptable for both species, albeit some absolute values, particularly in P1, presented remarkable deviations. The difference for each measuring point between the Original and the Modified configurations should be less pronounced than calculated as the experimental data suggested.

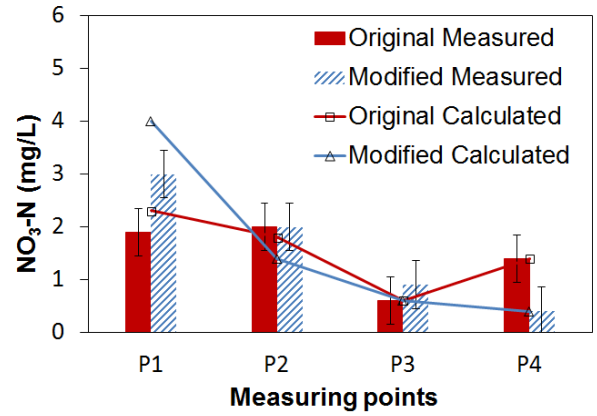

Figure 14. Comparison between nitrate concentration measured and calculated at both configurations

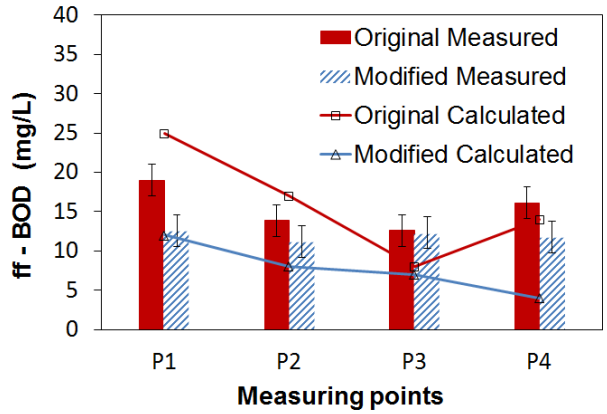

Figure 15. Comparison between filtered BOD measured and readily biodegradable substrate concentrations calculated at both configurations

Fitting full-scale sampling results obtained in a discrete way resulted particularly difficult. As explained in section 2.3.3, the majority of parameters for biokinetic model were taken from ASM1 default at 20ºC [10], but some of them such as the maximum specific growth rate and the decay coefficient for heterotrophic biomass, μ_H and b_H, were determined by respirometry with the objective to provide further information of the anoxic growth of heterotrophs resulting of 6.9 day^{-1} and 0.22 day^{-1}

respectively. Moreover, it was measured the half-saturation coefficient for heterotrophic biomass Ks = 4.9 gCOD m^{-3} since it is the main parameter influencing growth rate [32] and it presents a wider experimental value range compared with the other half-saturation default coefficients of Monod equations [27]. Yield for heterotrophic biomass (Y_H) resulted of 0.68 COD formed/COD oxidized. Dissolved oxygen concentration was measured continuously at different locations ensuring values below 0.1 mg/L within the anoxic zone.

Figures 17 and 18 show the comparison of nitrate and readily biodegradable substrate concentration distributions for the same scenario. The influence of the short-circuiting over the nutrient removal process can be noticed. Results show the improvement of the Modified configuration which provided lower nitrate concentration at the outcoming from the anoxic zone (Fig. 16) due to a better utilization of the organic matter for denitrification (Fig. 17).

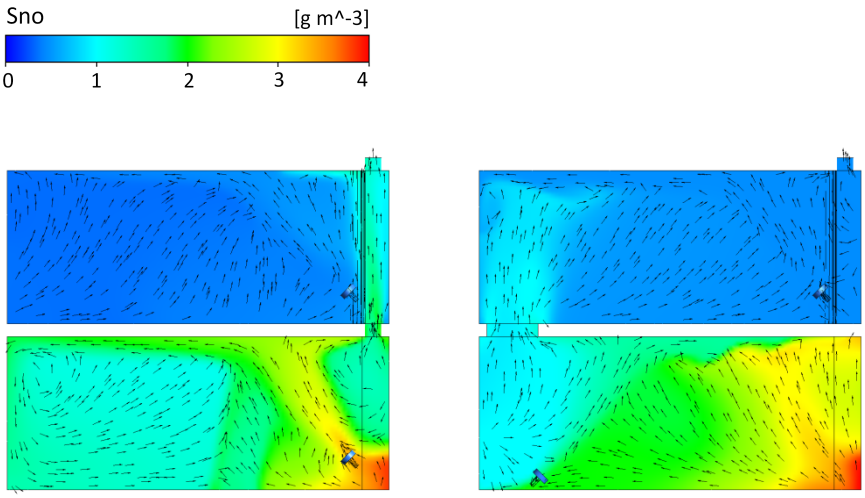

Figure 16. Nitrate (Sno) at Original configuration (left) and at Modified configuration (right)

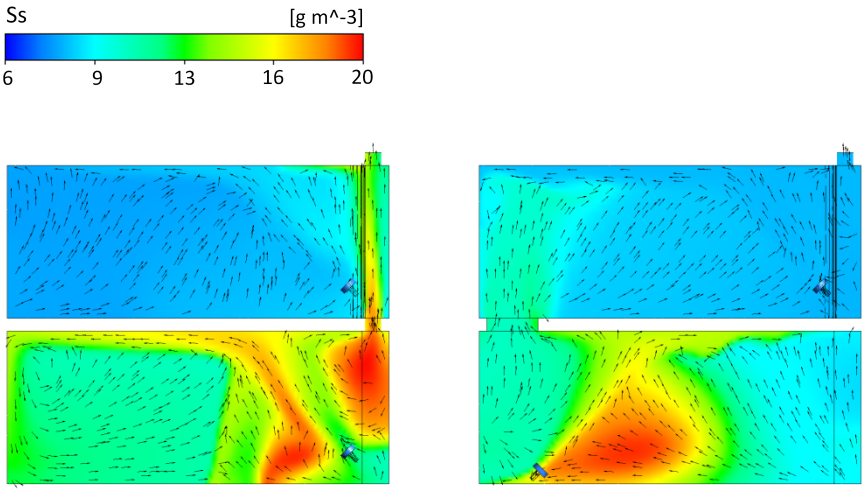

Figure 17. Readily biodegradable substrate (Ss) at Original configuration (left) and at Modified configuration (right)

Following the evaluation of CFD-ASM1 results and taking into account the complexity to show the CFD performances in 3D, the entire volume was divided into six virtual control cubicles. This analysis has been included as supplementary material providing biokinetic results from average values integrated in each subvolume. Results are shown by means of comparative histograms between both configurations. Figure 18 shows a noticeable improvement of the Sno performance for the Modified configuration which ensures low concentration at the outcoming anoxic flow and a better use of the available anoxic volume. The more plug-flow hydrodynamic behaviour from the retrofitting can be appreciated following the Sno value. The Original configuration showed the effect of the short-circuiting providing an undesirable high concentration at the outlet. Moreover, it exhibited locally high Ss values along the short-circuiting (Fig. 19). Because of the different hydrodynamics performance, consumption rates in the Original configuration offered the maximum values nearby the outlet (Figs. 20 and 21) which tended to worsen denitrification efficiency within the entire anoxic zone.

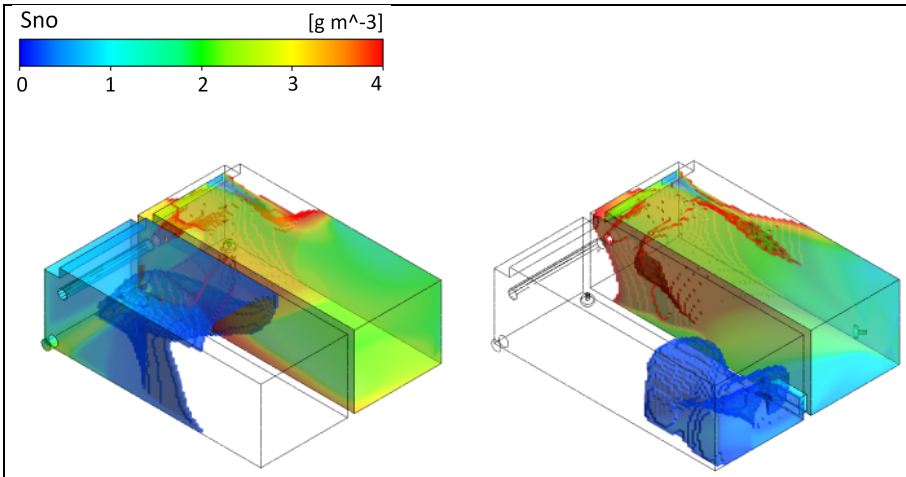

Figure 18**.** Nitrate (Sno) at Original configuration (left) and at Modified configuration (right).

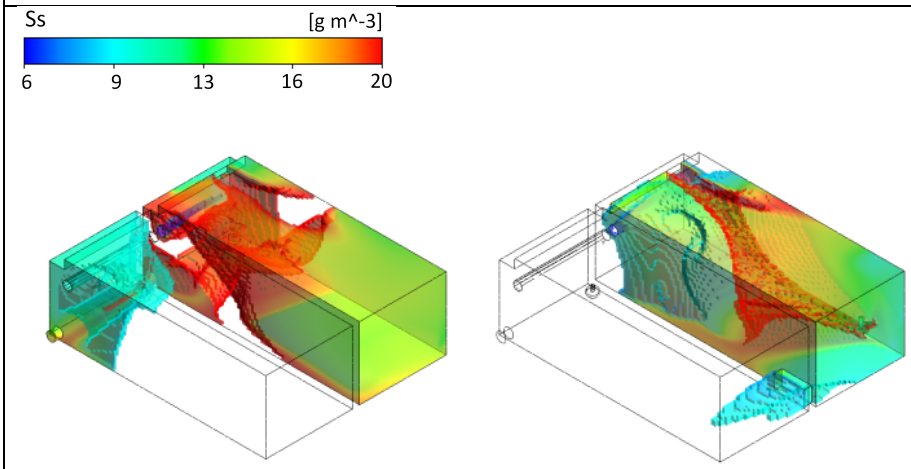

Figure 19. Readily biodegradable substrate (Ss) at Original configuration (left) and at Modified configuration (right).

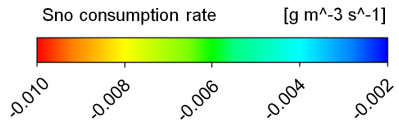

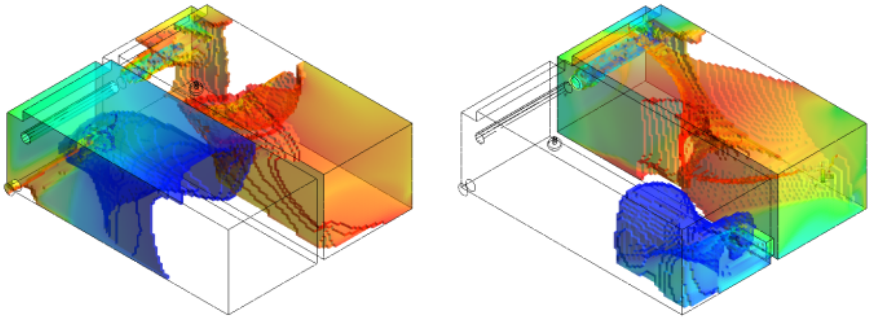

Figure 20. Nitrate consumption rate (g m^{-3} s^{-1}) at Original configuration (left) and at Modified configuration (right).

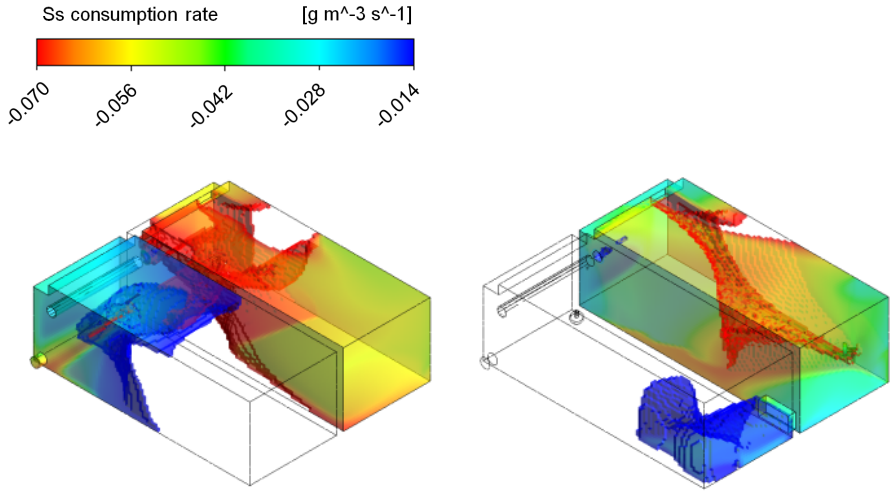

Figure 21. Readily biodegradable substrate consumption rate (g m^{-3} s^{-1}) at Original configuration (left) and at Modified configuration (right).

It is clear that CFD-ASM can provide a more faithful representation of the process, but as [12] pointed out, the complexity of the factors which depend on the reactor biomass-wastewater characteristics may provide more intricacy to adapt to a local approach such as CFD. Even so, results from CFD-ASM1 allowed evaluating changes in configuration in a full-scale tanks reproducing pollutant removal based on hydrodynamic performance.

4. Conclusions

CFD techniques can be successfully coupled with kinetic models as the ASM1 in order to provide a full description of the process within biological reactors. This coupling CFD-ASM permits to obtain detailed 3D velocity fields and biochemical compounds distributions. It is also possible to analyse the time evolution of these compounds distributions once they entry the reactor.

This work presents a case study using CFD-ASM1 to optimize the performance of a full-scale MLE biological reactor. The analysis of the reactor hydrodynamics revealed the strong influence of a short-circuiting in the anoxic zone on the overall behaviour. An alternative setup named Modified configuration, was proposed to avoid the short-circuiting. This configuration performance is based on the relocation of the wall-bushing and the stirrer. The CFD-ASM1 was used to optimize the shape and size of the wall-bushing and the location and the orientation of the stirrers in order to increase both the mean residence time and flow homogeneity, leading to an enhanced pollutant removal. The model was validated with experimental results for both Original and Modified configuration. Furthermore, a novel resolving scheme was proposed in order to significantly reduce the computational cost of the CFD-ASM simulations. The proposed approach consists on the solution of the steady state hydrodynamics followed by a transient simulation of compound transport that uses a specific time-stepping scheme. Several simulations were performed to show that this procedure provides with accurate results at a reduced time cost.

Acknowledgements

The authors would like to gratefully acknowledge the support provided by Entidad Pública de Saneamiento de Aguas Residuales (EPSAR).

References

[1] A. van Haandel, J. van der Lubbe, Handbook of Biological Wastewater Treatment: Design and optimization of Activated Sludge Systems, 2012.

[2] Metcalf & Eddy, Wastewater Engineering: Treatment and Reuse, 4th Editio, McGraw-Hill, 2004.

[3] C.D.M.F. P. Leslie Grady, Jr., Glen T. Daigger, Nancy G. Love, Biological Wastewater Treatment, Third, IWA Publishing, 2011.

[4] Water Environment Federation, Biological Nutrient Removal Processes, Oper. Munic. Wastewater Treat. Plants. (2007) 22-1-22–65.

[5] M. Brannock, Y. Wang, G. Leslie, Mixing characterisation of full-scale membrane bioreactors: CFD modelling with experimental validation, Water Res. 44 (2010) 3181–3191.

[6] T. Howes, M. Brannock, G. Corre, DEVELOPMENT OF SIMPLIFIED FLOW MODELS FROM CFD SIMULATIONS, (2003) 575–580.

[7] M. Brannock, Computational Fluid Dynamics Tools for the Design of Mixed Anoxic Wastewater Treatment Vessels PhD Thesis, University of Queensland, 2003.

[8] Y. Le Moullec, C. Gentric, O. Potier, J.P. Leclerc, CFD simulation of the hydrodynamics and reactions in an activated sludge channel reactor of wastewater treatment, Chem. Eng. Sci. 65 (2010) 492–498.

[9] J.I. Borroto, J. Domínguez, J. Griffith, M. Fick, J.P. Leclerc, Technetium-99m as a tracer for the liquid RTD measurement in opaque anaerobic digester: Application in a sugar wastewater treatment plant, Chem. Eng. Process. Process Intensif. 42 (2003) 857–865.

[10] M. Henze, W. Gujer, T. Mino, M.C.M. van Loosdrecht, Activated Sludge Models ASM1, ASM2, ASM2d and ASM3, IWA Publ. (2000) 121.

[11] J. Dudley, Process testing of aerators in oxidation ditches, Water Res. 29 (1995) 2217–2219.

[12] Y. Le Moullec, O. Potier, C. Gentric, J.P. Leclerc, Activated sludge pilot plant : Comparison between experimental and predicted concentration profiles using three different modelling approaches, 5 (2011).

[13] G.C. Glover, C. Printemps, K. Essemiani, J. Meinhold, Modelling of wastewater treatment plants - How far shall we go with sophisticated modelling tools?, Water Sci. Technol. 53 (2006) 79–89. doi:10.2166/wst.2006.078.

[14] A.M. Karpinska, J. Bridgeman, CFD-aided modelling of activated sludge systems e A critical review Standard Method of Moments, Water Res. 88 (2016) 861–879.

[15] J. Essemiani, K., Vermande, S., Marsal, S., Phan, L. and Meinhold, Optimisation of WWTP units using CFD – A tool grown for real scale application, (2004).

[16] R.W. Samstag, J.J. Ducoste, A. Griborio, I. Nopens, D.J. Batstone, J.D. Wicks, S. Saunders, E.A. Wicklein, G. Kenny, J. Laurent, CFD for wastewater treatment: An overview, Water Sci. Technol. 74 (2016).

[17] E. Wicklein, D.J. Batstone, J. Ducoste, J. Laurent, A. Griborio, J. Wicks, S. Saunders, R. Samstag, O. Potier, I. Nopens, Good modelling practice in applying computational fluid dynamics for WWTP modelling, Water Sci. Technol. 73 (2016).

[18] N. Eshtiaghi, F. Markis, S.D. Yap, J.C. Baudez, P. Slatter, Rheological characterisation of municipal sludge: A review, Water Res. 47 (2013). doi:10.1016/j.watres.2013.07.001.

[19] APHA/AWWA/WEF, Standard Methods for the Examination of Water and Wastewater, Stand. Methods. (2012) 541.

[20] ANSYS, ANSYS Academic Research, Release 16.2, Help System, Coupled Field Analysis Guide, ANSYS, Inc., (2015).

[21] F.R. Menter, Two-Equation Eddy-Viscosity Turbulence Models for Engineering Applications, AIAA J. 32 (1994) 1598–1605.

[22] E. Ramin, Modelling of secondary sedimentation under wet-weather and filamentous bulking conditions, (2014) 61.

[23] O. Potier, J.P. Leclerc, M.N. Pons, Influence of geometrical and operational parameters on the axial dispersion in an aereated channel reactor, Water Res. 39 (2005) 4454–4462.

[24] T. Casalini, M. Salvalaglio, G. Perale, M. Masi, C. Cavallotti, Diffusion and aggregation of sodium fluorescein in aqueous solutions, J. Phys. Chem. B. 115 (2011) 12896–12904.

[25] B. De Clercq, Fluid dynamics of settling tanks: development of experiments and rheological, settling, and scraper submodels, Ph.D. Thesis. (2003).

[26] F. Ghirelli, B. Leckner, Transport equation for the local residence time of a fluid, Chem. Eng. Sci. 59 (2004) 513–523.

[27] U. Jeppsson, G. Olsson, Modelling aspects of wastewater treatment processes, Dep. Ind. Electr. Eng. Autom. (1996) 444.

[28] J. Makinia, Mathematical Modelling and Computer Simulation of Activated Sludge Systems, IWA Publishing, London, 2010.

[29] O. Levenspiel, Chemical Engineering Reactor, John Wiey, New York, 1972.

[30] L.J. Burrows, A.J. Stokes, J.R. West, C.F. Forster, A.D. Martin, Evaluation of different analytical methods for tracer studies in aeration lanes of activated sludge plants, Water Res. 33 (1999) 367–374.

[31] L. Rieger, S. Gillot, G. Langergraber, T. Ohtsuki, A. Shaw, I. Takács, S. Winkler, Guidelines for Using Activated Sludge Models, IWA Publishing, London, 2013.

[32] M. Arnaldos, Y. Amerlinck, U. Rehman, T. Maere, S. Van Hoey, W. Naessens, I. Nopens, From the affinity constant to the half-saturation index: Understanding conventional modeling concepts in novel wastewater treatment processes, Water Res. 70 (2015) 458–470.